

Study of the reaction $pp \rightarrow pp\pi^0$ within 10 MeV above the threshold

COSY-TOF collaboration

S. AbdEl Samad^e, R. Bilger^d, A. Böhm^b, K.-Th. Brinkmann^b, H. Clement^d,
 S. Dshemuchadse^f, W. Eyrich^c, D. Filges^e, H. Freiesleben^b, M. Fritsch^c, R. Geyer^e,
 D. Hesselbarth^e, B. Jakob^b, K. Kilian^e, H. Koch^a, L. Karsch^b, J. Kress^d, E. Kuhlmann^{b#} ,
 S. Marwinski^e, P. Michel^f, K. Möller^f, H.P. Morsch^e, L. Naumann^f, M. Richter^b,
 E. Roderburg^e, M. Rogge^e, A. Schamlott^f, M. Schmitz^e, P. Schönmeier^b, M. Schroeder^c,
 M. Schulte-Wissermann^b, G.Y. Sun^b, M. Steinke^a, F. Stinzing^c, G.J. Wagner^d,
 M. Wagner^c, A. Wilms^a, S. Wirth^c

^a Institut für Experimentalphysik, Ruhr-Universität Bochum, D-44780 Bochum, Germany

^b Institut für Kern- und Teilchenphysik, Technische Universität Dresden, D-01062 Dresden, Germany

^c Physikalisches Institut, Universität Erlangen, D-91058 Erlangen, Germany

^d Physikalisches Institut, Universität Tübingen, D-72076 Tübingen, Germany

^e Institut für Kernphysik, Forschungszentrum Jülich, D-52425 Jülich, Germany

^f Institut für Kern- und Hadronenphysik, Forschungszentrum Rossendorf, D-01314 Dresden, Germany

November 27, 2002

Abstract

Kinematically complete measurements of the $pp \rightarrow pp\pi^0$ reaction were performed for beam energies in the range 292 – 298 MeV. By detecting both protons in coincidence with the large acceptance COSY-TOF spectrometer set up at an external beam line of the proton synchrotron COSY-Jülich, total and differential cross sections and energy distributions were obtained. A strong enhancement is observed in the Dalitz plots resulting from the final state interaction between the outgoing proton pair; the data are well reproduced by Monte Carlo simulations with standard parameters for scattering length $a_0 = -7.83$ fm and effective range $r_0 = 2.8$ fm. The total cross sections exceed the ones measured recently in internal target experiments at IUCF and CELSIUS by roughly 50 %. Arguments are presented which link this discrepancy with the effect of the final state interaction pushing yield into the very small-angle region and the near-impossibility of an internal target experiment to cover just this range.

PACS numbers: 13.75.Cs, 25.10.+s, 25.40.Ep, 29.20.Dh

corresponding author, e.kuhlmann@fz-juelich.de

I. Introduction

The last decade saw a renaissance of near-threshold pion producing reaction studies in nucleon-nucleon (NN) collisions. With the advent of medium-energy accelerators in Bloomington/USA (IUCF), Uppsala/Sweden (CELSIUS), and Jülich/Germany (COSY) a wealth of high precision data on total and differential cross sections as well as polarization observables was measured for the reactions $pp \rightarrow pp\pi^0$ [1-6], $pp \rightarrow pn\pi^+$ [7-9] and $pp \rightarrow d\pi^+$ [10-11], which in turn induced a flurry of theoretical activity [12-18]. So far, good agreement is found in the theoretical description of the reactions $pp \rightarrow d\pi^+$ and $pp \rightarrow pn\pi^+$, larger discrepancies are observed for the $pp \rightarrow pp\pi^0$ reaction. Soon after publication of the near-threshold data on neutral pion production it was recognized that the $pp\pi^0$ reaction near threshold is sensitive to short-range mechanisms in the NN-system. Since the main pion exchange term, which dominates the charged pion producing channels, is isospin-forbidden, Lee and Riska proposed to counter this shortfall by the additional consideration of pair diagrams with an exchanged heavy meson (σ, ω) [12]. Likewise the role of pion-rescattering only then was treated with more concern, but also in a somewhat controversial manner, since field theoretical models and chiral perturbation theories found different relative signs in the π -exchange amplitude with respect to the direct (Born) term [13], [14], [17]. Attempts have been pursued to additionally include $\Delta(1232)$ isobar and S_{11} and D_{13} nucleon resonance excitations [15-17]. To date, calculations in the framework of the Jülich meson exchange model [17], [18], which incorporate all the basic terms like heavy meson exchange (HME), delta resonance and off shell effects as well as realistic final-state interactions, yield the best results; with the exception of the strength parameter of the HME term the model needs no adjustable parameters.

Close to threshold only a few partial waves have to be considered with Ss, Sp, Ps and Pp being the leading ones, whereas the role of $l = 2$ contributions (Sd and Ds) is still under debate. Here the Rosenfeld notation $L_{NN}l_\pi$ has been used [19] with L_{NN} being the orbital angular momentum of the NN-pair, l_π that of the pion with respect to this pair. In the $pp\pi^0$ reaction the partial wave Sp which apart from Ss governs the isoscalar reaction channels $d\pi^+$ and $pn\pi^+$, is forbidden by conservation laws. As a result purely isotropic angular distributions are found for the $pp\pi^0$ reaction in the region up to 10 MeV above threshold [3]. Also, sizeable analyzing powers are only observed for this reaction for excess energies Q higher than 16 MeV [4] which follows from the fact that interference effects are only possible between amplitudes (Ps, Pp) on the one hand or (Ss,Sd,Ds) on the other. Except for Ss, however, the magnitude of all these amplitudes is negligibly small up to $Q = 16$ MeV.

For comparison, angular distributions as well as analyzing powers extracted from a study of the π^+ -producing reactions show clear evidence for the presence of Sp, and hence $l = 1$ contributions at energies as low as 2 MeV above threshold [10-11].

Measurements very close to threshold, where all escaping particles are confined to a narrow cone around the beam axis, require a perfectly matched detector system. Such a detector should cover as much of the available phase space as possible in order to reduce unavoidable, but necessary acceptance corrections to a minimum. In Jülich, the COSY-TOF spectrometer which is set up at an external beam line as a scintillator hodoscope of cylindrical shape with full ϕ -symmetry fulfills these requirements to a very large extend. Charged particles are detected at polar angles as close as one degree to the beam. In the past this spectrometer has successfully been used in meson- and hyperon-production studies and pp bremsstrahlung experiments. Parallel to the analysis of the bremsstrahlung reaction [20], data obtained simultaneously for $pp \rightarrow pp\pi^0$ were analysed as a cross check. We systematically found larger cross sections than given in [1], [3]. Since the results we deduced from the data for the concurring charged π -producing reactions agreed nicely with the published values [7], [10], [11], whereas the cross sections for π^0 -production remained high, we decided to perform a second experiment to clarify that matter.

In this paper we will present data from a kinematically complete measurement of the reaction $pp \rightarrow pp\pi^0$ for three energies in the range 292 - 298 MeV, corresponding to beam momenta of 796-805 MeV/c. Total cross sections as well as angular and energy distributions will be shown and compared to Monte Carlo simulations which are based on phase space distributed events that are modified by the final-state interaction (FSI). Results of the concurring reactions $pp \rightarrow d\pi^+$ and $pp \rightarrow pn\pi^+$ which were obtained in parallel will only be given to underline the performance of the spectrometer and to prove the consistency of the analysis. Apart from the excess energy Q we will also use the dimensionless parameter η for labelling energies above threshold defined as $\eta = q_{max}/m_\pi$ with q being the CM-momentum of the pion and m_π its mass. With p we denote the CM-momentum of one proton in the two-proton subsystem. The angles Θ_q and Θ_p (in the CM-system) are taken with respect to the beam. The momenta q and p are linked by energy conservation via $\sqrt{s} = \sqrt{m_\pi^2 + q^2} + \sqrt{M_{pp}^2 + q^2}$ and $M_{pp}^2 = 4(m_p^2 + p^2)$ where s is the square of the total CM energy and M_{pp} the invariant mass of the two protons.

II. Experimental Procedure

A. Apparatus

The experiment was carried out with the time-of-flight spectrometer COSY-TOF [21] [22] set up at an external beamline of the 2.5 GeV proton synchrotron COSY at Jülich/Germany. The goal was to study simultaneously and with the same spectrometer all five reaction channels which are open in pp-collisions at beam energies near 300 MeV. Besides pp-elastic scattering, which is by far the strongest, and the very weak pp bremsstrahlung, our interest mainly aimed at the π -producing reactions $pp \rightarrow d\pi^+$, $pp \rightarrow pp\pi^0$, and $pp \rightarrow pn\pi^+$, each one with cross sections rising fast with excess energy.

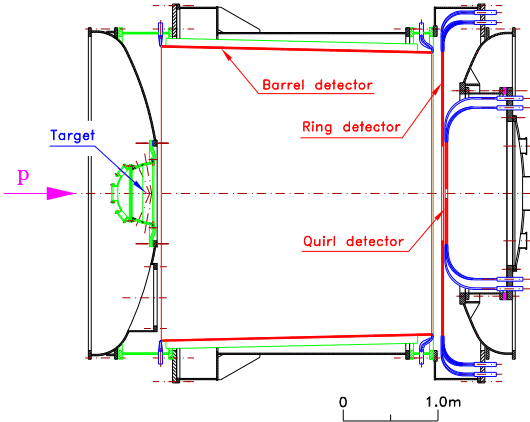


Figure 1: *Sketch of the COSY-TOF spectrometer*

A schematic sketch of the spectrometer showing the locations of the main components, the barrel (B), ring (R), and quirl (Q) detector, as well as the target region is given in fig. 1. To prevent the reaction products from undergoing secondary reactions on their way from the target to the different detector modules of the spectrometer it is housed within a $3.3 \text{ m} \times 4 \text{ m}$ steel tank which can be evacuated to a pressure of 0.2 Pa. Protons were extracted out of the COSY ring in a slow extraction mode allowing spill lengths of up to 10 min. Their intensity typically was of the order of several $10^6/\text{s}$. The beam was focussed onto the liquid hydrogen target with dimensions $6 \text{ mm} \times 4 \text{ mm}$ [23]. Its front and rear ends were closed by $0.9 \mu\text{m}$ thin hostaphan foils. A set of scintillator veto detectors with central holes of various sizes were located 260, 51 and 3.5 cm upstream of the target. They helped to define the beam spot in the center of the target to an area with diameter $d=3.0 \text{ mm}$. Charged particles emitted from the target into the forward hemisphere first had to transverse a 0.5 mm thin plastic scintillator set-up [24] placed right behind the target and serving as start

detector and then after a flight path of up to 3 m in vacuum, hit the 3-component (B, R, and Q) scintillator hodoscope. The start detector shown in fig. 2 consists of two concentric rings made out of 16 trapezoidally shaped scintillators each, the inner one having a central hole of diameter $d_i=3.3$ mm and extending out for 26 mm, and an outer one with dimensions $d_i=16$ mm and $d_a=130$ mm. The elements of the outer ring were arranged in such a way as to show a tiny overlap along their sides thus guaranteeing full ϕ -coverage whereas the ones of the inner ring were only allowed to touch each other thereby leaving narrow gaps of order $50 \mu\text{m}$ which caused an overall loss in ϕ -coverage of 3 % distributed evenly over the full circle.

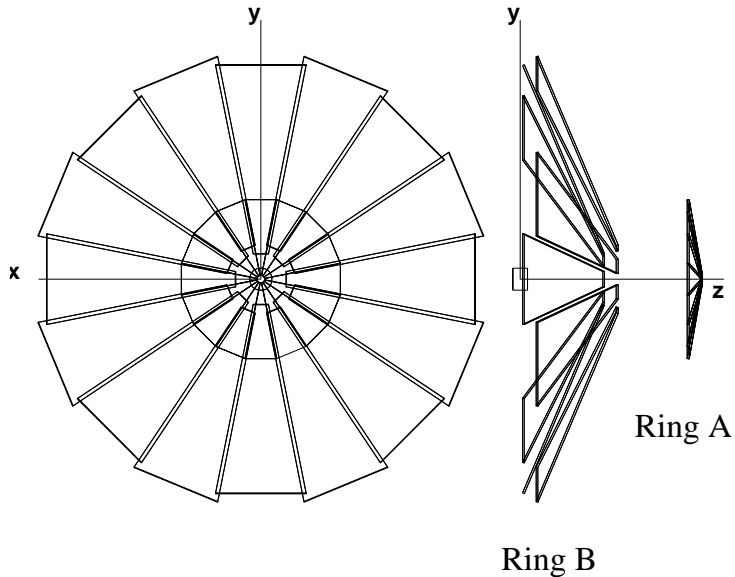


Figure 2: *Front and side view of the start detector*

The circular, 3-layer quirl and ring detector components of the endcap were both built according to the same layout. 5 mm thin scintillator sheets (BC408) were used as basic material. The first layer in the quirl is made from 48 wedge-like scintillators, followed by two layers with 24 left and 24 right wound elements, each element cut along an Archimedian spiral [21]. In central projection a net-like pattern is formed consisting of more than 1000 triangular pixels. A central hole of radius $r=4.2$ cm was left for the beam, the outer radius of the quirl is 58 cm. The three layers in the ring were made from 96 wedges and 2×48 left and right wound Archimedian spirals, the inner (outer) radius is 56.8 (154) cm, respectively. The barrel consists of 96 scintillator bars, mounted to the inside of the tank. Each bar of

2.85 m length has a cross section with measures thickness \times width = 15 mm \times 96 mm and is read out from both ends [22].

In the course of the experiment which went on for almost two years two slightly different set-ups were employed. The one described above with barrel, ring and quirl was used at $T=293.5$ MeV. Azimuthal coverage was complete, the acceptance in polar angle θ ranged from $1.5^\circ - 78^\circ$. In an earlier experiment performed at $T=292.2$ and 298.1 MeV the ring component was still under construction, leaving a gap in polar angle θ between $10.3^\circ - 26^\circ$. For this run a modular neutron detector [25] was additionally set up downstream around the beam line and outside of the tank. It covered approximately the same area as the quirl detector and was employed in the study of the concurring $pp \rightarrow pn\pi^+$ reaction. As a first level trigger usually one, in some cases two charged hits were required in the start detector, at least two in any of the stop detectors B, R, Q, with 2B, 2R, 2Q and 2(BRQ) denoting separately handled trigger patterns. For each of these patterns slightly different deadtimes were observed and the necessary corrections had to be applied accordingly.

B. Performance Checks and Luminosity Monitor

Simultaneously with the π -producing reactions, elastic scattering events, which were detected either as barrel-barrel (BB) or as barrel-ring (BR) coincidences, were written on tape. In addition to serving as a tool for calibrating the whole detector system, this reaction was used as a luminosity monitor through comparison of experimentally deduced elastic scattering events with data taken from the SAID database [26] (see fig. 3). The cross section around $T = 300$ MeV is known with an error of less than 5 %. Any cross section of interest determined relative to the one for pp_{elast} will thus be measured with comparable accuracy, since all uncertainties resulting from instabilities in beam intensity and target thickness cancel.

Complementary information on the detector performance was obtained from a careful study of the $pp \rightarrow d\pi^+$ -reaction. Its cross section at 295 MeV is close to $45 \mu b$ [10] thus yielding comparable statistical accuracy for this reaction compared to the other pion channels. While the deuterons will only reach the quirl, the pions with $\theta^{max} = 32^\circ$ can be observed in all of the three stop-detector components. The unique kinematics of this 2-particle reaction allowed extremely narrow cuts in the offline analysis thus producing rather clean and almost background free spectra as e.g., invariant d - and π^+ -mass distributions. In plotting the experimentally obtained transverse π -momentum p_t versus the longitudinal π -momentum p_l and using two-body kinematics, the energy of the extracted beam could be deduced with

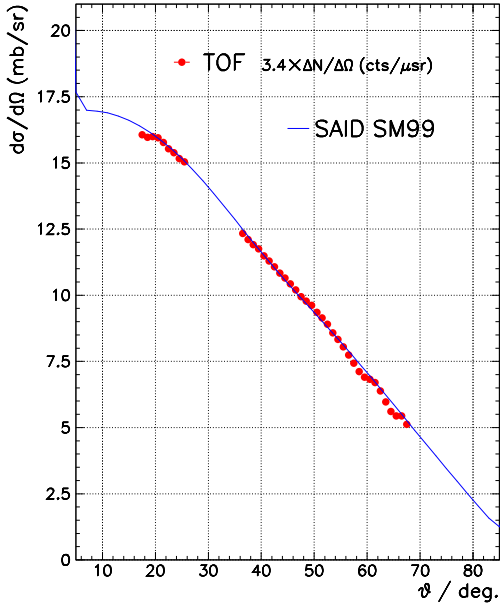


Figure 3: *Measured angular distribution of elastic pp scattering events (data points) compared to the SAID solution (full line, see text)*

high precision to be $T_p = 293.5 \pm 0.3$ MeV. In fig. 4 the dashed line in the middle corresponds to the quoted beam energy, the two solid lines have been calculated for beam energies which are 0.6 MeV higher and lower.

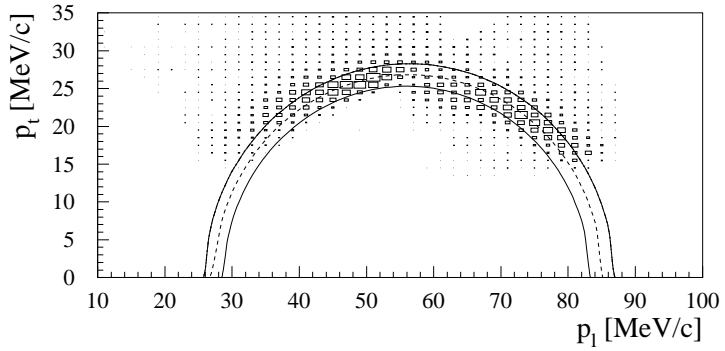


Figure 4: *Transverse vs. longitudinal π -momentum in comparison with expectations from two-body kinematics for various beam energies (see text for details)*

III. Data Analysis and Calibration

A. Principle of Measurement

The photomultiplier signals of all detector elements were used for energy-loss as well as time-of-flight measurements. To this end, the analog signals were digitized in Fastbus-QDC

modules, the timing signals were derived in leading-edge type discriminators and used in Fastbus TDCs. Both measurements yield the particle velocity β . From the particle's point of impact the flight direction was obtained from which two additional observables, θ and ϕ , can be derived. In the endcap with its 3-layer quirl and ring components the flight direction is deduced by combinatorical means [21]. For the one-layer barrel elements with two-sided readout the point of impact is found from the difference in TDC-values of both ends [22], whereas the TDC-sum is a measure of the flight time. The spatial resolution as given from the pixel size in the endcap is $\Delta\theta = 0.5^\circ$, $\Delta\phi = 4^\circ$; roughly the same values hold for the barrel elements. Typical values obtained for the time resolution of the start-stop system were of the order of 0.5 ns (FWHM) which corresponds to about 2.5 % of the average flight time of a $\beta = 0.5$ particle.

The momentum 4-vector of each detected particle can then be deduced from the measured observables β , θ , and ϕ by applying an additional mass hypothesis. This of course has to be checked in comparison with results obtained from Monte Carlo simulations. In case of a reaction with one neutral particle like $pp \rightarrow pp\pi^0$ the 4-vector of that particle is deduced by employing energy and momentum conservation and calculating its missing mass.

B. Calibration

In order to determine θ , ϕ and β for each particle, several steps in calibrating the detector had to be performed [27]. After a simple pedestal subtraction in the QDC spectra, a walk correction had to be applied for each TDC entry. Depending on the pulse height of the scintillator signal, time shifts of up to 3 ns were observed. To correct for these shifts a five-parameter fit function was found which relates the observed walk with the pulse height given by the corrected QDC value. The complete parameter list for up to 600 scintillator channels was determined before each experiment. This was routinely done by use of a laser-based calibration system where UV-light from a N_2 -laser is fed via quartz fibers into each of the individual scintillator channels. Through use of a set of filters the amount of light going into the various elements can be varied such as to cover the complete dynamic range of the multipliers.

A check on the differential nonlinearity in the TDC modules revealed no deviations from the precision given by the manufacturer (< 0.1 % of full scale), in some cases, however, a channel width of 90 ps/channel only was observed instead of the preset value of 100 ps/channel. Due to different cable lengths and varying transit times in the photomultiplier tubes and electronic modules, variations in the signal arrival time arise which are specified

as TDC-offsets. These offsets were determined in an iterative manner by first comparing overlapping, but otherwise identical channels as e.g., neighboring elements in the outer start detector (sect. II.A) or overlap regions from left- and right-wound elements in the endcap. Two-particle reactions like pp_{elast} and $d\pi^+$ with their unique kinematics then were used for the adjustment of all remaining detector components. As a byproduct the light velocities within the differently shaped scintillator elements were deduced. Whereas in bulk material it is given by c/n (n : index of refraction), smaller values were found for the rather flat, but long elements due to an effective lengthening of the lightpath. For the straight quirl elements of wedgelike shape and a thickness of 5 mm we found 18.0 cm/ns, for the corresponding ones of the ring 15.8 cm/ns. A value of 16.1 cm/ns was observed for the 3 m barrel elements. The calibration of the neutron detector was performed as outlined in [25]. Special care was applied in the determination of the energy-dependent efficiency which, for neutron energies larger than 60 MeV, was found to be rather constant around 13.5 %.

C. Monte Carlo simulation

Throughout the analysis each step was compared to the results deduced from the Monte Carlo simulation. The program package was set up with the purpose of simulating the spectrometer response, thereby giving insight into the overall performance, and to determine the detector acceptance. At its core is the CERNLIB random event generator GENBOD [28], which generates a preset number of N-body events for a given reaction specified by N, the number of ejectiles, their masses and the 4-momentum of the incoming beam. It returns momentum 4-vectors for each particle in the overall center of mass system, and weight factors w_{ps} based on the phase space density of the reaction. These weight factors have to be modified, if angular momentum or final-state interaction effects are known to play a substantial role. The Monte Carlo code then boosts this event into the laboratory system and each particle is tracked through the complete setup. Great care was put into modelling all of the detector components in their particular shape as close as possible to reality, including the left- and right-wound spirals in the endcap and the trapezoidal elements of the slightly conical barrel detector. Options were built into the program to study in detail the influence of the extended target and the transverse beam spread or the variation in acceptance due to the narrow gaps between neighboring scintillator elements or the size of the central hole in the inner start detector.

In the course of the simulation, interactions of the particles on their way through the various active or passive detector parts can be switched on or off, their energy loss and small-

angle scattering can be investigated separately. Effective low-energy thresholds can thus be studied in detail as eg., in case of the endcap, where a hit in at least two layers is needed for a successful pixel reconstruction. Also included in the Monte Carlo package is the possibility of particle decay. In the present case it was found that a sizeable fraction of the π^+ -mesons with low momentum had decayed before the detector was reached and a decay myon was detected instead.

IV. Results

A. Total cross sections

By use of energy and momentum balance, the $pp\pi^0$ events were identified by calculating the missing mass m_x of the unobserved neutral pion according to

$$m_x^2 = (\mathbb{P}_b + \mathbb{P}_t - \mathbb{P}_1 - \mathbb{P}_2)^2,$$

where $\mathbb{P}_b(\mathbb{P}_t)$ denote the beam (target) momentum 4-vector, respectively, and \mathbb{P}_i the one of the i-th proton. The high energy part of the distribution obtained at $T = 293.5$ MeV is given in fig. 5 showing a clear signal at the expected location $m_x = m_\pi = 0.134$ GeV/c^2 .

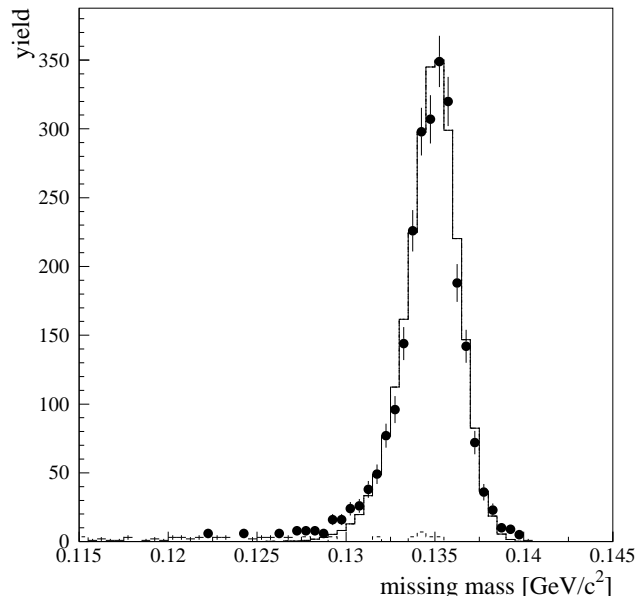


Figure 5: *Missing-mass spectrum of reconstructed $pp\pi^0$ -events (dots with error bars) in comparison with the Monte Carlo simulation (histogram). The dashed histogram shows the normalized spectrum obtained with an empty target.*

Table 1: *Total $pp \rightarrow pp\pi^0$ cross sections derived at three beam energies. The column labelled acc lists the detector acceptance as determined from our Monte Carlo simulations based on FSI modulated phase space distributed events.*

T (MeV)	η	N_π	acc	$\int L dt$ (nb $^{-1}$)	σ_{tot} (μb)
292.2 ± 0.3	0.29	1586	0.55	1.25	$2.31 \pm 0.06 \pm 0.23$
293.5 ± 0.3	0.30	2524	0.64	1.41	$2.80 \pm 0.06 \pm 0.21$
298.1 ± 0.2	0.35	4426	0.49	2.43	$3.72 \pm 0.06 \pm 0.28$

The only cuts applied in the analysis were upper limits on the β -values of the protons in order to eliminate events where a much faster pion was wrongly interpreted as a proton. Background due to reactions on the target foils or condensates thereon is negligible as can be seen from the spectrum obtained from an empty target run and shown by the dashed histogram in fig. 5. Also displayed is the result of our Monte Carlo simulation (solid histogram) which is in excellent agreement with the data. Summing up the events for $m_x \geq 0.13 \text{ GeV}/c^2$ and making minute corrections for falsely interpreted $pp \rightarrow pn\pi^+$ -events of order 3 % from Monte Carlo considerations, one finds the number of $pp\pi^0$ -events as given in column 3 of table 1. Column 4 lists the acceptances as derived from our Monte Carlo simulations. The main deviation from complete acceptance ($acc \equiv 1$) results from geometrical properties as e.g., the central hole in the inner start detector (mainly for the low-energy measurements) and the missing ring component (see sect. II.A) for the measurement at $T=298.1$ MeV. Nevertheless, in all cases acceptance values of order 50 % or higher were found. The integrated luminosities as given in column 5 of table 1 were derived from a comparison with the results obtained for pp-elastic scattering in the angular range $32^\circ - 55^\circ$, a range that was covered by the barrel alone. For the measurement at $T=293.5$ MeV, where the ring was available as well, the quoted value not only is corroborated by the results found for the extended range $18^\circ - 70^\circ$, but also from a comparison with results for $pp \rightarrow d\pi^+$. For this reaction a total cross section of $\sigma = 42 \pm 5 \mu b$ was found in very good agreement with an interpolated value of $44 \mu b$ deduced from [29].

Total cross sections for the reaction $pp \rightarrow pp\pi^0$ are given in the last column of table 1 together with their statistical and systematical errors. The latter are composed of 5 % from the pp cross section, 3.5 % from the acceptance correction, 1.5 % from the uncertainty in misinterpreted background events and 2 % in the luminosity determination.

B. Dalitz Plots and Energy Distribution

As mentioned before, a crucial point in the determination of the total cross section is the extrapolation of the measured data into the full region allowed by phase space. A thorough understanding of the detector response is essential, as is the knowledge of any deviation in the original (physical) data from those given by simple phase space, i.e. s-wave distributed

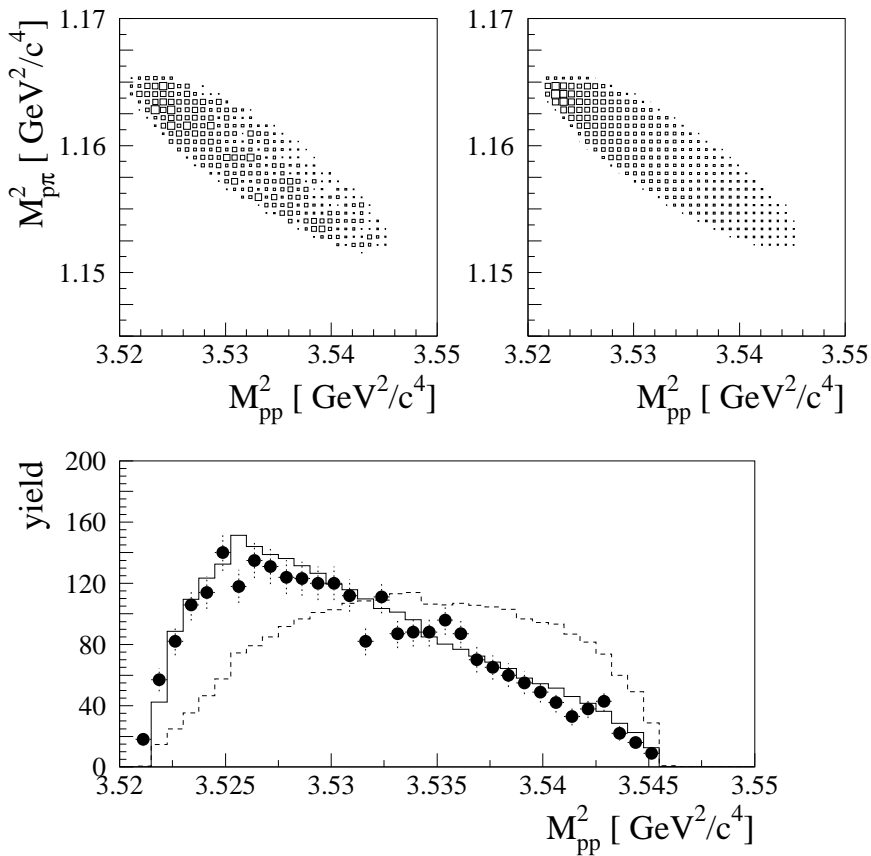


Figure 6: *top:* Dalitz plots of experimental (left) and simulated (right) data. The enhancement due to FSI is seen in the upper left corner of the event distribution. *bottom:* projection of the Dalitz plots onto the M_{pp}^2 -axis. Experimental data are given by solid dots with statistical error bars, the solid histogram shows the simulated distribution. The dashed histogram represents the simulated distribution for pure phase space.

events. A convenient way to compare in a comprehensive manner experimental and simulated data from a 3-particle reaction is to set up a Dalitz plot, which quite instructively allows the extraction of the underlying physics from the event distribution. Purely phase space distributed events will result in a uniformly covered Dalitz plot, any deviation thereof will induce some modulations. The Dalitz plot as found from the present (kinematically fitted) data at $T=293.5$ MeV is shown in fig. 6 and compared to the result of our Monte Carlo simulation (top row left and right, respectively). As a consequence of the strong final state interaction in the pp system a systematic enhancement in the top left corner is observed in the data. The simulated distribution was obtained by incorporating the FSI formalism as developed in [30], [31] and later refined by Morton et al. [32]. In short, one calculates additional weight factors w_{fsi} which are multiplied with the event weight w_{ps} given by the CERNLIB subroutine GENBOD (see also sect. III.C). These factors are given as

$$w_{fsi} = C^2 \cdot [C^4 \cdot T_{pp}^{CM} + \frac{(\hbar c)^2}{m_p c^2} \left(\frac{m_p c^2}{2(\hbar c)^2} r_0 \cdot T_{pp}^{CM} - \frac{1}{a_0} - \sqrt{2} \frac{\alpha m_p c^2}{\hbar c} \cdot h(\gamma_q) \right)^2]^{-1},$$

where T_{pp}^{CM} denotes the pp center of mass kinetic energy $T_{pp}^{CM} = M_{pp} - 2m_p$ and C^2 the Coulomb penetration factor

$$C^2 = \frac{2\pi \cdot \gamma_q}{e^{2\pi \gamma_q} - 1}$$

with $\gamma_q = \frac{\alpha \cdot \mu_{pp} \cdot c}{q_{pp}}$. Here α is the fine structure constant, $q_{pp} = \sqrt{2\mu_{pp} T_{pp}^{CM}}$ and μ_{pp} is the reduced mass of the pp-system. The term with $h(\gamma_q) = \gamma_q^2 \cdot \sum_n \frac{1}{n(n^2 + \gamma_q^2)} - 0.5772 - \ln \gamma_q$ contributes only little and is often omitted. From literature we took the standard values $a_0 = -7.83$ fm and $r_0 = 2.8$ fm [33] as input parameters for the scattering length and effective range, respectively, for the two protons in the 1S_0 state. The smooth rise in yield which readily is seen in the simulated data is partially obscured in the experimental data due to the limited statistical accuracy. However, when inspecting the projection of the 2-dimensional Dalitz plot distribution onto the x-axis it is obvious that only through inclusion of FSI effects the simulated data follow the experimental ones (fig. 6, bottom) whereas a simulation based on purely phase space distributed events fails over the whole range.

The proton energy distribution T_{pp}^{CM} at 293.5 MeV in the center of mass system is shown in fig. 7. That close to threshold proton energies only range up to roughly 7 MeV with a very distinct maximum near 1 MeV. The FSI-based simulation given by the dashed histogram reproduces the data very well, whereas a simple phase space distribution (given by the dotted histogram and normalized to the experimental yield) fails completely. Also shown is the result of a simulation where final state interaction effects have been included but with

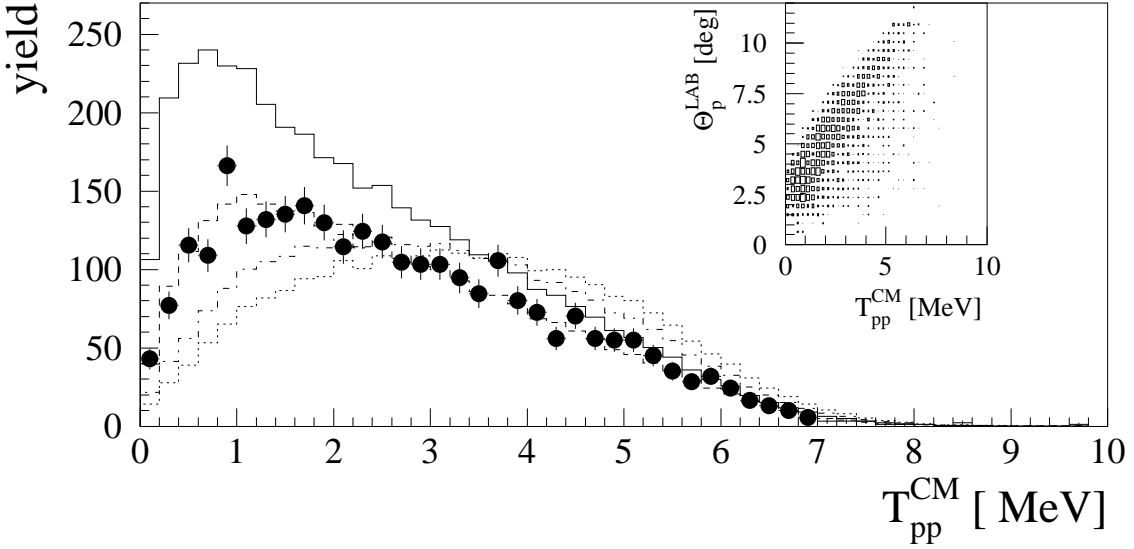


Figure 7: Proton energy distribution T_{pp}^{CM} in the 2-proton CM system (solid dots with statistical error bars) in comparison with the Monte Carlo simulation including FSI with standard parameters (dashed histogram). The extrapolation to full acceptance is shown by the solid histogram. The pure phase space distribution is given by the dotted histogram, a simulation with FSI and a scattering length $a_0 = -1.5 \text{ fm}$ by the dash-dotted histogram. The insert shows Θ_p^{LAB} , the smaller of the two proton angles, vs. T_{pp}^{CM} (see text).

a much reduced scattering length of $a_0 = -1.5 \text{ fm}$ as was suggested in [4] (fig. 7, dash-dotted histogram). When normalizing this distribution to our experimental data as was done in fig. 7 very poor agreement is observed. If on the other hand one normalizes only to the upper part beyond $T_{pp}^{CM} = 3.0 \text{ MeV}$ the maximum around 1.0 MeV is totally missed and we cannot see how a proper extrapolation can be achieved. From the insert showing in a two-dimensional plot Θ_p^{LAB} , the smaller of the two proton angles, versus T_{pp}^{CM} , it can be seen, that the maximum yield found near $T_{pp}^{CM} = 1 \text{ MeV}$ is connected with one of the two protons emerging towards Θ -values well below 5° , a range that is almost completely without detector coverage in each of the two internal target experiments. In view of this observation we argue that an extrapolation towards full acceptance can only be performed correctly by using the standard values $a_0 = -7.83 \text{ fm}$ and $r_0 = 2.8 \text{ fm}$ as scattering length and effective range, respectively. The result is given by the solid histogram in fig. 7.

C. Angular Distribution

Acceptance corrected angular distributions for the pion- and relative two-proton-momentum vectors are shown in fig. 8 for the measurement at $T=293.5$ MeV. The solid lines are the result of fits in terms of Legendre polynomials P_l to the experimental data $W(\cos\Theta) \propto 1 + \sum_l a_l \cdot P_l(\cos\Theta)$ up to $l = 2$. Only very small a_2 -coefficients were found as expected that close to threshold, namely $a_2 = +0.05 \pm 0.10$ for the top and $a_2 = +0.08 \pm 0.11$ for the bottom distribution. Similar results were obtained at the other two bombarding energies. The observed symmetry around $\cos\Theta = 0$ (or the vanishing of the P_1 -term) which stems from the entrance channel consisting of two identical particles was not used as a constraint in the fit; instead we consider it as a valuable check on the quality of our acceptance corrections.

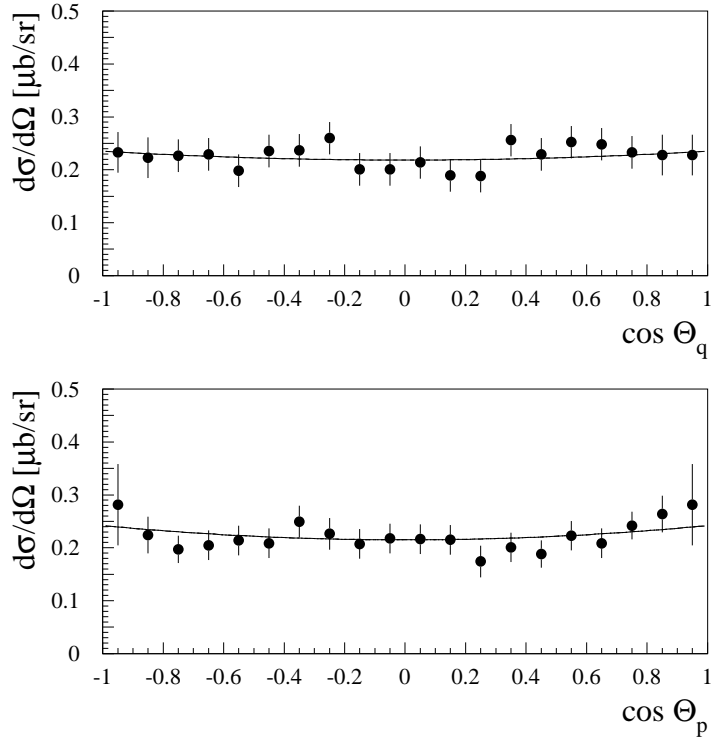


Figure 8: Acceptance corrected angular distributions in $\cos\Theta_q$ (direction of pion momentum) and $\cos\Theta_p$ (direction of relative two-proton momentum) in the CM system as obtained at $T = 293.5$ MeV. The solid lines are the result of Legendre polynomial fits up to $l = 2$.

The angular distribution obtained for the $pp \rightarrow pn\pi^+$ reaction at $T=298.1$ MeV corresponding to $\eta = 0.19$ was found to be consistent with isotropy which is in agreement with the published data [8]. Sizeable anisotropies were found for the angular distribution of the 2-particle reaction $pp \rightarrow d\pi^+$ yielding an a_2 -coefficient of order $+0.2$ and larger with, however, an error of comparable size. This is a consequence of the significant acceptance corrections

which had to be performed to account for those pions which had decayed before reaching the detector, as well as those which were too low in momentum as being able to reach the second layer of the endcap (see also sect. III.C).

IV. Discussion

The total cross sections listed in table 1 are compared to results found in the literature [1-3], [5-6] in fig. 9. In the range $\eta = 0.2 - 1.0$ σ rises over two orders of magnitude up to values close to $100 \mu\text{b}$. The present data exceed the ones from IUCF and CELSIUS by roughly 50 %. This discrepancy we connect with the one basic difference in experimental set-up, namely theirs being an internal, ours, however, an external target experiment. The most critical step in extracting an absolute cross section lies in the acceptance correction, which depends on the knowledge of i) geometrical coverage of the available phase space, ii) angular distribution effects, and iii) deviations from s-wave distributed events due to final

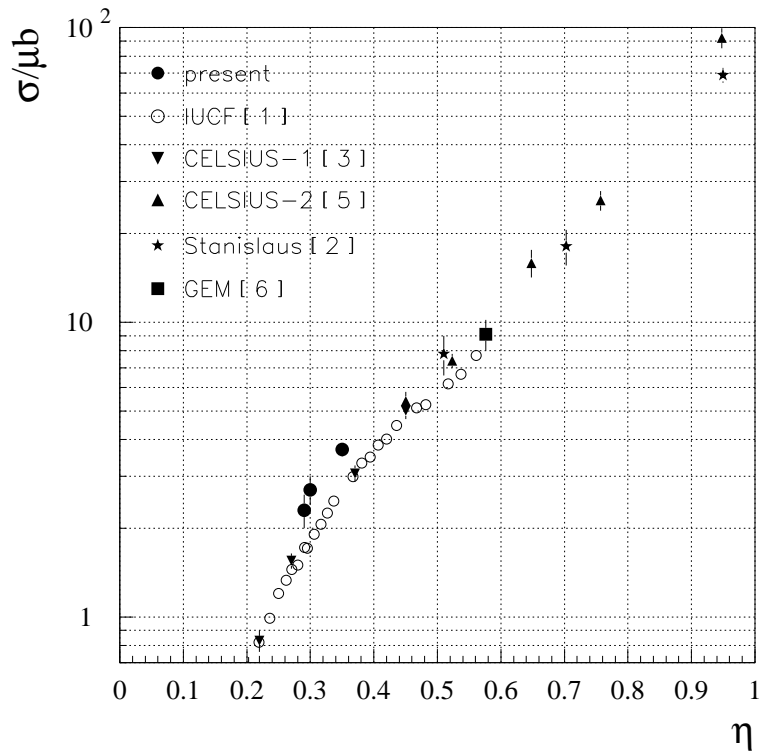


Figure 9: *Summary of cross section data as known today for $pp \rightarrow pp\pi^0$ up to $\eta = 1.0$. The present data given by thick dots clearly are higher than the earlier ones from IUCF (open circles, [1]) and CELSIUS (solid downward triangles, [3]).*

state effects. Since, most probably, the geometrical coverage is well accounted for in all three cases, and angular distribution effects are negligible, we believe a poor treatment of the strong FSI effects to be responsible for the large discrepancy. Our reasoning is as follows: The lower the energy above threshold, the more important the relative weight of FSI becomes, and, simultaneously, the more yield gets compressed into the very small angle region. If on the other hand the minimum angle is only near 4° , as is the case in the internal target experiments at IUCF [1] or CELSIUS [3], [5], more and more yield is missed. To extrapolate into the uncovered region requires a very profound knowledge of the original distribution, and most often some model dependence will enter the extrapolation procedure. As was mentioned before the data given in [1] were corrected by using non-standard FSI parameters (scattering length $a_0 = -1.5$ fm) which completely failed to reproduce the present data. The low-energy CELSIUS-data [3] were obtained by detecting the two decay photons instead of the two emerging protons, a method with an acceptance which is only weakly dependent on excess energy and is free of any threshold effects, but suffers from the very small geometric coverage of only 5 %. To perform the acceptance correction for the high-energy CELSIUS data [5] a rather elaborate procedure has been developed which at the same time was meant to account for FSI- and angular distribution effects. Obviously a stronger model dependence is involved. When comparing their published acceptance-corrected and -uncorrected momentum distributions for data obtained at the lowest energy point at 310 MeV (figs. 13 and 14 of ref. [5]) a drastic shape change is observed, which hints at the strong effect of the acceptance correction. In the present study the extrapolated distribution is much less different from the original one as can be seen from fig. 7, and thus, to our opinion, more reliable.

A summary of Legendre polynomial expansion coefficients a_2 found in the literature for the pion producing reactions in the near threshold region is shown in fig. 10 as a function of η . Three bands of data are discernible. The fastest rise with η is observed for the $pp \rightarrow d\pi^+$ reaction (given by open symbols, refs. [10 – 11], [34]) where deviations from $a_2 = 0$ are already found below $\eta = 0.1$. The positive a_2 -coefficients are an indication for strong p-wave contributions. Much less information is available for the other π^+ -producing reaction measured at IUCF and TRIUMF and plotted as asterisks [8] and diamonds [35], respectively. Yet a comparable behaviour of a fast rise can be observed as well, which, however, only starts somewhat later near $\eta = 0.2$. For both these reactions with an isoscalar two-nucleon pair in the exit channel the Sp partial wave which is not Pauli forbidden contributes almost from threshold. A totally different pattern is observed in case of the $pp \rightarrow pp\pi^0$ -reaction. Near-

isotropy is found for almost the whole η -range shown in fig. 10 with a_2 staggering between -0.2 and +0.2 and only developing some unique trend toward positive values for $\eta > 0.9$. It is not clear whether d-wave contributions which induce negative a_2 coefficients might be present that close to threshold.

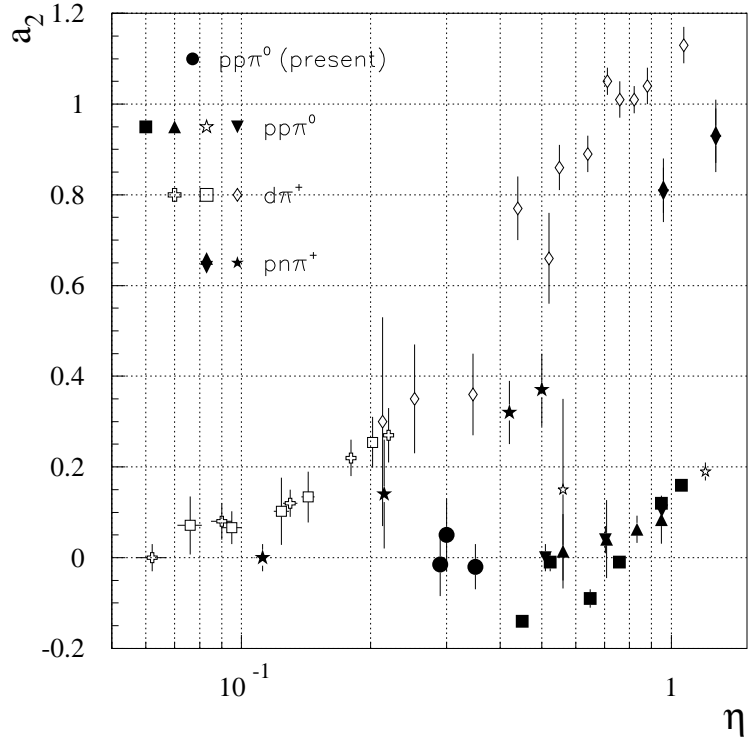


Figure 10: *Comparison of experimental a_2 -coefficients as obtained from Legendre polynomial fits to π -angular distributions in the near threshold region. $pp \rightarrow d\pi^+$ -data are given by open symbols, the ones for $pp \rightarrow pn\pi^+$ by solid stars and diamonds. Solid dots, squares and triangles as well as open asterisks are used to denote the data for $pp \rightarrow pp\pi^0$ (see text).*

Up to approximately $\eta = 0.7$ the Ss partial wave alone by far dominates the $pp\pi^0$ -reaction. As was pointed out in [17] the cross section in this region could only be reproduced satisfactorily when adding to the coherent sum of direct and rescattering term, which make up roughly 60 % of the measured yield, an extra heavy meson exchange (HME) contribution with a “free” strength parameter. Yet at energies above $\eta = 1$ where higher partial waves start to contribute significantly and where Δ -isobar contributions were additionally considered the predictions nevertheless underestimate the data. In view of the present findings of a much larger cross section also at low η values which would require an even larger strength parameter for HME contributions it might be conceivable that something more essential is

missing in the theoretical description of the near-threshold $pp\pi^0$ reaction. It seems to be worth mentioning that poor agreement is also found in recent calculations of polarization observables [36].

V. Summary

The $pp \rightarrow pp\pi^0$ reaction has been investigated in a kinematically complete experiment by detecting the two protons in the large acceptance spectrometer COSY-TOF set up on an external beam line of the proton synchrotron COSY. Total cross sections were obtained at bombarding energies of 292.2, 293.5 and 298.1 MeV, which exceed previous measurements by roughly 50 %. Invariant mass and energy distributions are governed by strong final state effects. The importance of detecting protons well below 4° to the beam line is stressed. The angular distributions for the pion and relative two-proton momentum vectors were found to be nearly isotropic as expected that close to threshold.

Some results were also presented for the concurring charged pion producing reactions $pp \rightarrow d\pi^+$ and $pp \rightarrow pn\pi^+$.

Acknowledgements

The help of the COSY crew in delivering a low-emittance proton beam is gratefully acknowledged. The data are based in part on the analysis work performed by B. Jakob [27]. We like to thank R. Klein and M. Würschig-Pörsel for their continued assistance in solving technical problems. Helpful discussions with C. Hanhart are very much appreciated. Financial support was granted by the FFE fund of the Forschungszentrum Jülich and by the German BMBF.

References

- [1] H.O. Meyer et al., Nucl. Phys. **A539** (1992) 633
- [2] S. Stanislaus et al., Phys. Rev. **C44** (1991) 2287
- [3] A. Bondar et al., Phys. Lett. **B356** (1995) 8
- [4] H.O. Meyer et al., Phys. Rev. **C63** (2001) 064002
- [5] R. Bilger et al., Nucl. Phys. **A693** (2001) 633
- [6] M. Betigeri et al. (GEM collaboration), Phys. Rev. **C65** (2002) 064001
- [7] J.G. Hardie et al., Phys. Rev. **C56** (1997) 20
- [8] R.W. Flammang et al., Phys. Rev. **C58** (1998) 916
- [9] W.W. Daehnick et al., Phys. Rev. **C65** (2002) 024003
- [10] M. Drochner et al., Phys. Rev. Lett. **77** (1996) 454
- [11] P. Heimberg et al., Phys. Rev. Lett. **77** (1996) 1012
- [12] T.-S. Lee and D.O. Riska, Phys. Rev. Lett. **70** (1993) 2237
- [13] B.-Y. Park et al., Phys. Rev. **C53** (1996) 1519
- [14] T.D. Cohen et al., Phys. Rev. **C53** (1996) 2661
- [15] U. Van Kolck et al., Phys. Lett. **B388** (1996) 679
- [16] M.T. Peña et al., Phys. Rev. **C60** (1999) 045201
- [17] C. Hanhart et al., Phys. Lett. **B444** (1998) 25
- [18] C. Hanhart et al., Phys. Rev. **C61** (2000) 064008
- [19] A.H. Rosenfeld, Phys. Rev. **96** (1954) 130
- [20] R. Bilger et al., Phys. Lett. **B429** (1998) 195
- [21] M. Dahmen et al., Nucl. Inst. and Methods in Phys. Res. **A348** (1994) 97

- [22] A. Böhm et al., Nucl. Inst. and Methods in Phys. Res. **A443** (2000) 238
- [23] A. Hassan et al., Nucl. Inst. and Methods in Phys. Res. **A425** (1999) 403
- [24] P. Michel et al., Nucl. Inst. and Methods in Phys. Res. **A408** (1998) 453
- [25] L. Karsch et al., Nucl. Inst. and Methods in Phys. Res. **A460** (2001) 362
- [26] R.A. Arndt et al., Phys. Rev. **C50** (1994) 2731
- [27] B. Jakob, Ph.D. Thesis, Technische Universität Dresden (2001)
- [28] GENBOD, CERN Program Library Long Write-up W515 (1993)
- [29] M. Drochner et al., Nucl. Phys. **A643** (1998) 55
- [30] K.M. Watson, Phys. Rev. **88** (1952) 1163
- [31] A.B. Migdal, Sov. Phys. JETP **1** (1955) 2
- [32] B.J. Morton et al., Phys. Rev. **169** (1968) 825
- [33] H.P. Noyes, Ann. Rev. Nuclear Science **22** (1972) 465
- [34] B.G. Ritchie et al., Phys. Rev. Letters **66** (1991) 568
- [35] R.G. Pleydon et al., Phys. Rev. **C59** (1999) 3208
- [36] C. Hanhart, Proceedings MESON2002, Krakow/Poland (2002), nucl-th/0207015